INORGANIC CHEMISTRY FRONTIERS

RESEARCH ARTICLE

View Article Online
View Journal | View Issue

Cite this: *Inorg. Chem. Front.*, 2022, **9**, 5616

Assembly of cyclic ferrocene-sensitized titanium-oxo clusters with excellent photoelectrochemical activity†

Chao Wang, * Ning Chen, Shoujuan Wang and Fangong Kong

The development of crystalline titanium-oxo clusters has made great progress in recent years. However, the geometric assembly of titanium-oxo clusters is still very challenging. Herein, we report the assembly of two cyclic titanium-oxo clusters with ferrocene connectors, formulated as $Ti_{12}(\mu_3\text{-}O)_4(Fcdc)_4(O^iPr)_{32}\cdot 0.5CH_2Cl_2$ (Fcdc = 1,1′-ferrocenedicarboxylic acid; **$Ti_{12}Fcdc_4$**) and $Ti_{18}(\mu_2\text{-}O)_6(\mu_3\text{-}O)_6(Fcdc)_2(L1)_2(L2)_4(O^iPr)_{34}\cdot 2HO^iPr$ (L1 = isonicotinic acid; L2 = salicylhydroxamic acid; **$Ti_{18}Fcdc_2$**). Single-crystal X-ray diffraction studies demonstrate that ferrocene with two carboxylic arms can adhere to the surface of $\{Ti_6\}$ and/or $\{Ti_3\}$ units, resulting in fascinating cyclic structures of **$Ti_{12}Fcdc_4$** and **$Ti_{18}Fcdc_2$**. Notably, ferrocene ligands can not only serve as connectors to induce the geometric assembly of Ti-oxo clusters, but can also act as photosensitizers to greatly improve the light absorption behavior of the resulting compounds. Furthermore, the DFT calculation results suggest that the HOMO → LUMO transition mainly involves ferrocenyl group → Ti-oxo core charge transfer. Using the two ferrocene-containing clusters as electrode precursors, both electrodes exhibited excellent photocurrent responses. Our work opens a new way for the geometric assembly of titanium-oxo clusters and also contributes to the deep understanding of the structure–property relationships of sensitized Ti-based materials.

Received 8th May 2022,
Accepted 31st August 2022

DOI: 10.1039/d2qi01007k

rsc.li/frontiers-inorganic

Introduction

Recently, crystalline titanium-oxo cluster materials have attracted a significant amount of attention.[1–8] The main motivation not only comes from their potential applications in photocatalysis and photoelectric conversion, but also lies in their accurate atomic structure which is beneficial for theoretical calculations and mechanism studies.[9–14] In the past decade, crystalline titanium-oxo clusters have achieved rapid growth in their structural library.[15–25] Although some attractive titanium-oxo cluster architectures were assembly synthesized and characterized by X-ray diffraction,[26–35] such as cages, prisms, and cyclic structures, the rational design and geometric assembly of titanium-oxo clusters is still very challenging. Various synthesis parameters, including temperature, reactant ratio, solvent, and coordinating ligands, will directly affect the assembly of titanium-oxo clusters.[36–40] Among them, the coordinating ligands as one of the most important raw materials play crucial roles in the assembly of titanium-oxo clusters.[41–49]

The metallocene-based molecule 1,1′-ferrocenedicarboxylic acid ($FcdcH_2$) is a potential coordinating ligand. The $FcdcH_2$ connector can display multiple conformations formed by the different angles between the carboxylate groups, which can be helpful for the assembly of complexes with fascinating geometries.[50–52] Additionally, ferrocene-containing complexes, which are a class of potential excellent photoelectric materials, usually show narrow band gaps and excellent photoelectric responses.[53–55] However, as far as we know, only a few titanium-oxo clusters with $FcdcH_2$ ligands have been reported to date, and they also show broad light absorption and efficient charge transfer.[56–58] Based on the above considerations, we hope to effectively regulate the structural geometry and light absorption of titanium-oxo clusters by employing $FcdcH_2$ as a bridging ligand, thereby realizing the controllable assembly and photoelectric applications of titanium-oxo clusters containing ferrocene connectors.

Herein, we successfully synthesized two cyclic titanium-oxo clusters with $FcdcH_2$ connectors, formulated as $Ti_{12}(\mu_3\text{-}O)_4(Fcdc)_4(O^iPr)_{32}\cdot 0.5CH_2Cl_2$ (Fcdc = 1,1′-ferrocenedicarboxylic acid; **$Ti_{12}Fcdc_4$**) and $Ti_{18}(\mu_2\text{-}O)_6(\mu_3\text{-}O)_6(Fcdc)_2(L1)_2(L2)_4(O^iPr)_{34}\cdot 2HO^iPr$ (L1 = isonicotinic acid; L2 = salicylhydroxamic acid; **$Ti_{18}Fcdc_2$**). Single-crystal X-ray diffraction studies demonstrate

State Key Laboratory of Biobased Material and Green Papermaking, Qilu University of Technology (Shandong Academy of Sciences), Jinan, 250353, China.
E-mail: wangchao@qlu.edu.cn

†Electronic supplementary information (ESI) available. CCDC 2164045(1) and 2164046(2). For ESI and crystallographic data in CIF or other electronic format see DOI: https://doi.org/10.1039/d2qi01007k

that the {Ti_6} and/or {Ti_3} units are connected by bridging $FcdcH_2$ connectors to generate fascinating cyclic structures of **$Ti_{12}Fcdc_4$** and **$Ti_{18}Fcdc_2$**. We found that ferrocene ligands can not only serve as connectors to induce the assembly of titanium-oxo clusters, but can also act as photosensitizers to greatly improve the light absorption behavior of the resulting compounds. The DFT calculation results suggest that the HOMO → LUMO transition mainly involves ferrocenyl group → Ti-oxo core charge transfer. Using the two compounds as electrode precursors, both electrodes exhibited excellent photocurrent responses.

Experimental

Synthesis of $Ti_{12}(\mu_3\text{-}O)_4(Fcdc)_4(O^iPr)_{32}\cdot 0.5CH_2Cl_2$ (1, $Ti_{12}Fcdc_4$)

To a 23 mL Teflon-lined autoclave were added 55 mg of $FcdcH_2$ (0.2 mmol) and 3 mL of CH_2Cl_2, and then 100 μL of $Ti(O^iPr)_4$ (0.3 mmol) was added. After stirring for 10 min, the mixture was transferred to an oven at 100 °C for 72 h. After cooling, red crystals of **$Ti_{12}Fcdc_4$** were obtained (76% yield based on Ti $(O^iPr)_4$). IR data (cm^{-1}): 1633 (m), 1491 (s), 1394 (s), 1358 (m), 1194 (m), 1029 (w), 924 (w), 787 (m), 618 (w), 576 (w), 521 (w).

Synthesis of $Ti_{18}(\mu_2\text{-}O)_6(\mu_3\text{-}O)_6(Fcdc)_2(L1)_2(L2)_4(O^iPr)_{34}\cdot 2HO^iPr$ (2, $Ti_{18}Fcdc_2$)

To a 23 mL Teflon-lined autoclave were added 55 mg of $FcdcH_2$ (0.2 mmol), 77 mg of salicylhydroxamic acid (0.5 mmol), 62 mg of isonicotinic acid (0.5 mmol), and 5 mL of isopropanol, and then 100 μL of $Ti(O^iPr)_4$ (0.3 mmol) was added. After stirring for 10 min, the mixture was transferred to an oven at 100 °C for 72 h. After cooling, yellow crystals of **$Ti_{18}Fcdc_2$** were obtained (68% yield based on $Ti(O^iPr)_4$). IR data (cm^{-1}): 1600 (s), 1577 (m), 1509 (s), 1399 (s), 1358 (w), 1312 (w), 1267 (m), 1249 (w), 1194 (w), 1157 (w), 1102 (w), 1033 (m), 920 (w), 763 (m), 677 (m), 613 (m), 521 (w).

Results and discussion

Syntheses

Crystals of **$Ti_{12}Fcdc_4$** and **$Ti_{18}Fcdc_2$** were obtained by a solvothermal reaction. Fig. 1 displays the crystal pictures of **$Ti_{12}Fcdc_4$** and **$Ti_{18}Fcdc_2$**. During synthesis, we found that the solvent has an important effect on the assembly synthesis of **$Ti_{12}Fcdc_4$**. When dichloromethane was replaced by isopropanol, only a microcrystalline sample could be obtained. As for the synthesis of **$Ti_{18}Fcdc_2$**, salicylhydroxamic acid as an auxiliary ligand plays a significant role in the reaction system. If there is no salicylhydroxamic acid, only a solution sample could be obtained. For the discussion of the molecular structures, intrinsic characteristics, and photoelectric behaviors of these two Ti-oxo clusters containing ferrocene connectors, see the following sections.

Structures

X-ray single crystal diffraction analysis reveals that **$Ti_{12}Fcdc_4$** crystallizes in the orthorhombic system, space group *Pbcn*, and the structure of **$Ti_{12}Fcdc_4$** consists of twelve Ti^{4+} ions, four $Fcdc^{2-}$ connectors, four $\mu_3\text{-}O^{2-}$, thirty-two $-O^iPr^-$ ions, and half a free CH_2Cl_2 molecule. In the structure of **$Ti_{12}Fcdc_4$**, three Ti atoms are linked by one μ_3-O atom to form a planar triangle $[Ti_3(\mu_3\text{-}O)]^{10+}$ unit, and four $[Ti_3(\mu_3\text{-}O)]^{10+}$ units are connected by four bridging $Fcdc^{2-}$ linkers to form a closed-loop structure of **$Ti_{12}Fcdc_4$** (Fig. 1b and S1†). Notably, the two carboxylate groups of each $Fcdc^{2-}$ connector present an angle of 142.76°, and each carboxylate group was coordinated to two Ti atoms in the $[Ti_3(\mu_3\text{-}O)]^{10+}$ unit. Except for the $Fcdc^{2-}$ groups, the outer surface of each $[Ti_3(\mu_3\text{-}O)]^{10+}$ unit is surrounded by two bridging isopropyl groups and six terminal isopropyl groups. In the $[Ti_3(\mu_3\text{-}O)]^{10+}$ unit, Ti1 and Ti2 (Ti4 and Ti5) atoms are six-coordinated in an octahedral environment, while the Ti3 (Ti6) atom is five-coordinated in a hexahedral environment (Fig. 1c). Furthermore, the space-filling structure and packing structure of **$Ti_{12}Fcdc_4$** are shown in Fig. 2a and b. The distance between the two adjacent $[Ti_3(\mu_3\text{-}O)]^{10+}$ units in **$Ti_{12}Fcdc_4$** is about 4.98 Å.

X-ray single crystal diffraction analysis revealed that **$Ti_{18}Fcdc_2$** crystallizes in the triclinic system, space group $P\bar{1}$. In the structure of **$Ti_{18}Fcdc_2$**, two $[Ti_3(\mu_3\text{-}O)]^{10+}$ units and two $[Ti_6(\mu_2\text{-}O)_3(\mu_3\text{-}O)_2]^{14+}$ units are connected by two $Fcdc^{2-}$ and two isonicotinic acid connectors, resulting in the rectangular structure of **$Ti_{18}Fcdc_2$** (Fig. 1e and S2†). The two carboxylate groups of each $Fcdc^{2-}$ connector present an angle of 135.47°, and four O atoms of the $Fcdc^{2-}$ linker were coordinated with Ti1, Ti2 in the $[Ti_3(\mu_3\text{-}O)]^{10+}$ unit and Ti4, Ti5 in the $[Ti_6(\mu_2\text{-}O)_3(\mu_3\text{-}O)_2]^{14+}$ unit, respectively. One N atom and two O atoms of isonicotinic acid were coordinated to Ti4 in the $[Ti_6(\mu_2\text{-}O)_3(\mu_3\text{-}O)_2]^{14+}$ unit and Ti2, Ti3 in the $[Ti_3(\mu_3\text{-}O)]^{10+}$ unit, respectively. The two salicylhydroxamic acid ligands are attached to each $[Ti_6(\mu_2\text{-}O)_3(\mu_3\text{-}O)_2]^{14+}$ unit. Moreover, the outer surface of each $[Ti_6(\mu_2\text{-}O)_3(\mu_3\text{-}O)_2]^{14+}$ unit is surrounded by nine isopropyl groups, involving three bridging isopropyl groups and six terminal groups. In the $[Ti_6(\mu_2\text{-}O)_3(\mu_3\text{-}O)_2]^{14+}$ unit, all the Ti atoms except for the Ti8 atom show octahedral TiO_6 coordination environments, while the Ti8 atom is five-coordinated in a hexahedral environment (Fig. 1f). Also, the space-filling structure and packing structure of **$Ti_{18}Fcdc_2$** are shown in Fig. 2c and d. The length and width of the rectangles in **$Ti_{18}Fcdc_2$** are about 4.96 and 4.29 Å, respectively.

The X-ray diffraction (XRD) patterns of **$Ti_{12}Fcdc_4$** and **$Ti_{18}Fcdc_2$** are in good agreement with those simulated from the crystallographic data (Fig. S5 and S6†), indicating the phase purity of the samples. Thermogravimetric analysis (TGA) showed that **$Ti_{12}Fcdc_4$** and **$Ti_{18}Fcdc_2$** have similar thermal behaviour, and the two cluster frameworks remain stable up to approximately 200 °C (Fig. S7 and S8†). The infrared spectroscopy (IR) spectra of **$Ti_{12}Fcdc_4$** and **$Ti_{18}Fcdc_2$** are shown in Fig. S9 and S10.† The vibrational bands in the range of 600–700 cm^{-1} can be attributed to Ti–O–Ti vibrations, while the vibrational bands in the range of 1000–1100 cm^{-1} correspond to Ti–O–C vibrations. The vibration observed at around 1500 cm^{-1} belongs to the characteristic vibrations of the ferrocene groups. To identify the chemical state of the elements in

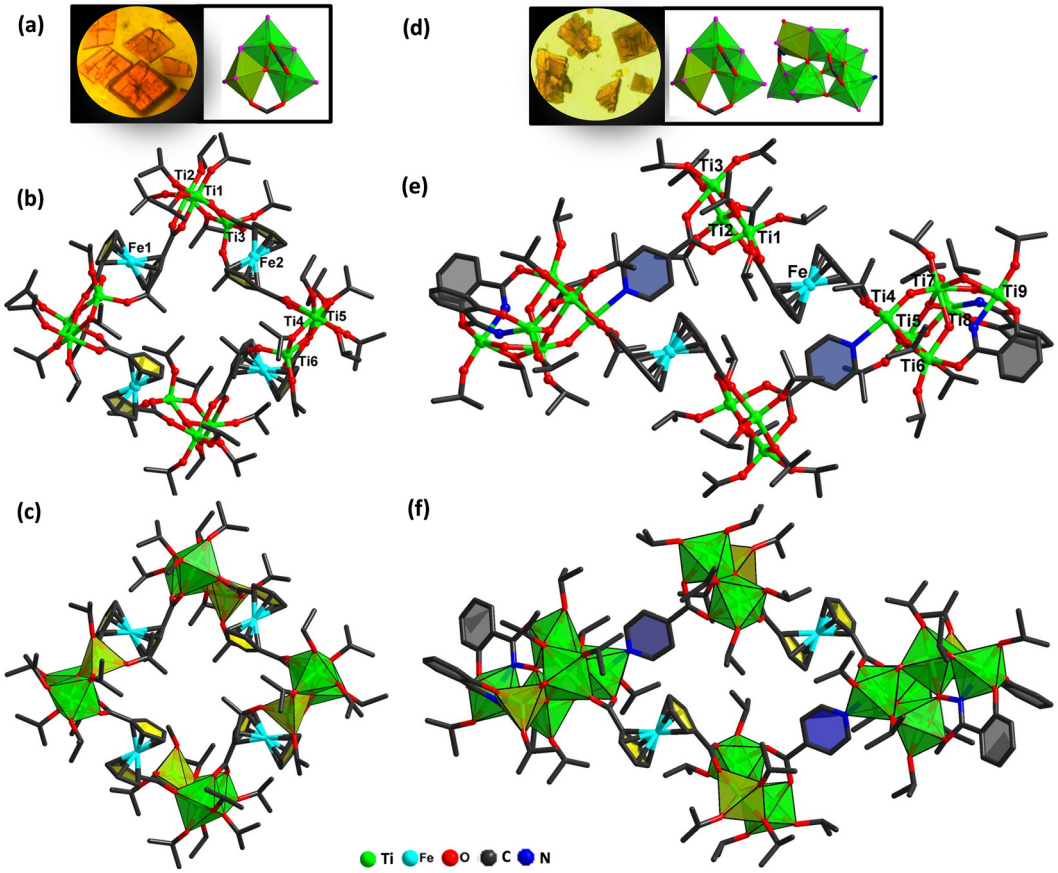

Fig. 1 (a) Crystal photograph of $Ti_{12}Fcdc_4$; inset is the {Ti_3} unit of $Ti_{12}Fcdc_4$. (b) Ball–stick view of $Ti_{12}Fcdc_4$. (c) Polyhedral view of $Ti_{12}Fcdc_4$. (d) Crystal photograph of $Ti_{18}Fcdc_2$; insets are {Ti_3} and {Ti_6} units of $Ti_{18}Fcdc_4$. (e) Ball–stick view of $Ti_{18}Fcdc_2$. (f) Polyhedral view of $Ti_{18}Fcdc_2$.

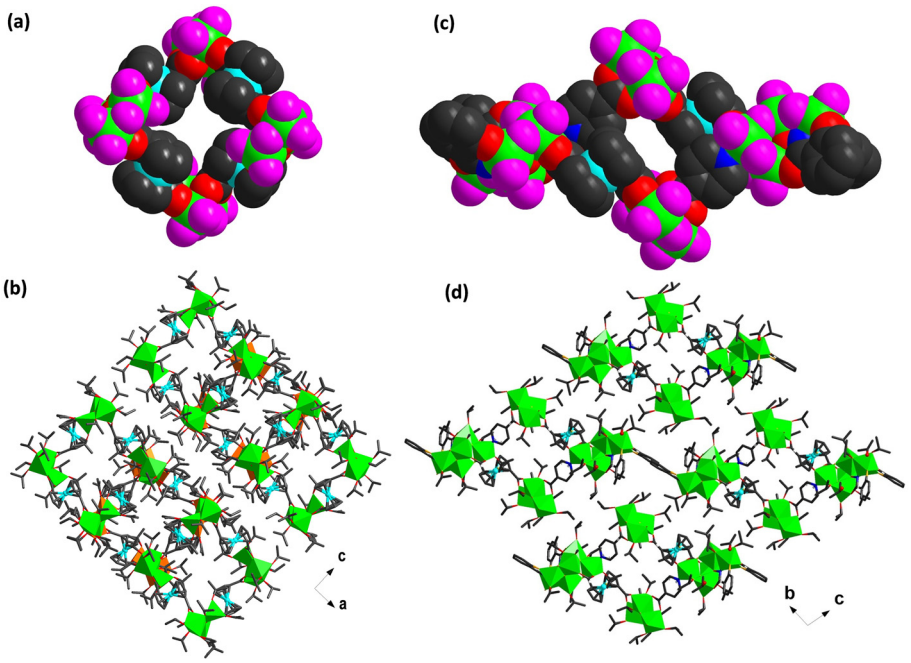

Fig. 2 Space-filling structure and packing structure of $Ti_{12}Fcdc_4$ (a and b) and $Ti_{18}Fcdc_2$ (c and d).

$Ti_{12}Fcdc_4$ and **$Ti_{18}Fcdc_2$**, X-ray photoelectron spectroscopy (XPS) analysis was carried out. Fig. S11† shows the Ti 2p and Fe 2p regions of the high resolution XPS spectra. There were two signal peaks located at 458.8 and 464.6 eV, corresponding to Ti $2p_{3/2}$ and Ti $2p_{1/2}$, respectively, which confirms the existence of a Ti^{4+} cation. The pair of binding energies existing at 708.1 and 720.7 eV correspond to Fe $2p_{3/2}$ and Fe $2p_{1/2}$, indicating the presence of an Fe^{2+} cation.

Light absorption behaviors

To evaluate the light absorption of these compounds, UV-vis absorption spectrum analysis was carried out. As shown in Fig. 3a, **$Ti_{12}Fcdc_4$** and **$Ti_{18}Fcdc_2$** display broad absorption bands with an absorption edge at about 600 nm, which is similar to previously reported ferrocene-sensitized Ti-oxo clusters.[55,57,58] The ultraviolet absorption is mainly ascribed to the $O_{2p} \rightarrow Ti_{3d}$ charge transfer transitions in titanium-oxo clusters.[2,4] The remarkable visible absorption bands of **$Ti_{12}Fcdc_4$** and **$Ti_{18}Fcdc_2$** can be mainly attributed to the charge transfer transition from the ferrocenyl groups to the Ti-oxo cores. The band gaps of **$Ti_{12}Fcdc_4$** and **$Ti_{18}Fcdc_2$** were calculated to be about 2.05 and 2.11 eV, respectively, from the absorption band edge (Fig. 3b). Actually, both **$Ti_{12}Fcdc_4$** and **$Ti_{18}Fcdc_2$** display lower band gaps than pure Ti-oxo clusters. The narrow band gap may be explained by the contribution from charge transfer between the Fcdc ligands and the Ti-oxo cores.

Density functional theory (DFT) calculations

Theoretical DFT calculations based on the crystal data were performed to further investigate the charge transfer transition process of **$Ti_{12}Fcdc_4$** and **$Ti_{18}Fcdc_2$**. For **$Ti_{12}Fcdc_4$**, the electron densities of the highest occupied molecular orbitals (HOMO to HOMO−3) are mainly assigned to the Fe 3d orbitals of the ferrocenyl groups, and the lowest unoccupied molecular orbitals (LUMO to LUMO+3) are predominantly dominated by contributions from the Ti 3d orbitals of the Ti-oxo core (Fig. 4a). The DFT calculation results suggest that the HOMO → LUMO transition mainly involves the charge transfer from the ferrocenyl groups to the Ti-oxo cores. For **$Ti_{18}Fcdc_2$**, most coefficients of the HOMO, HOMO−2 and HOMO−3 are located on the salicylhydroxamic acid and $FcdcH_2$ ligands, and the LUMO, LUMO+2 and LUMO+3 are mainly located on the Ti-oxo core and isonicotinic acid (Fig. 4b). This result suggests that for **$Ti_{18}Fcdc_2$**, the HOMO → LUMO electron transition can mainly correspond to the charge transfer from the salicylhydroxamic acid and Fcdc ligands to the Ti-oxo cores.

Photoelectrochemical (PEC) measurements

To investigate the carrier charge transfer efficiency, we measured transient photocurrent responses of these Ti-oxo

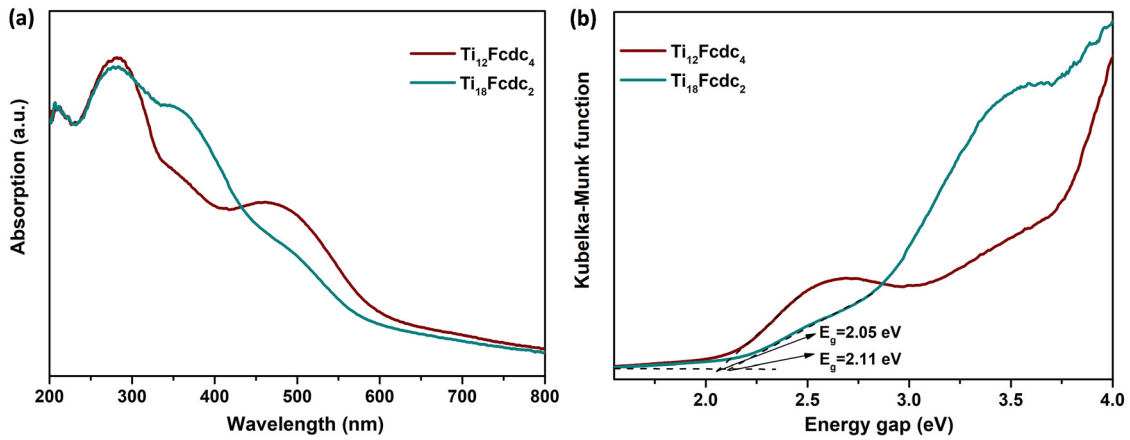

Fig. 3 (a) Solid-state UV/vis absorption spectra and (b) the band gaps of **$Ti_{12}Fcdc_4$** and **$Ti_{18}Fcdc_2$**.

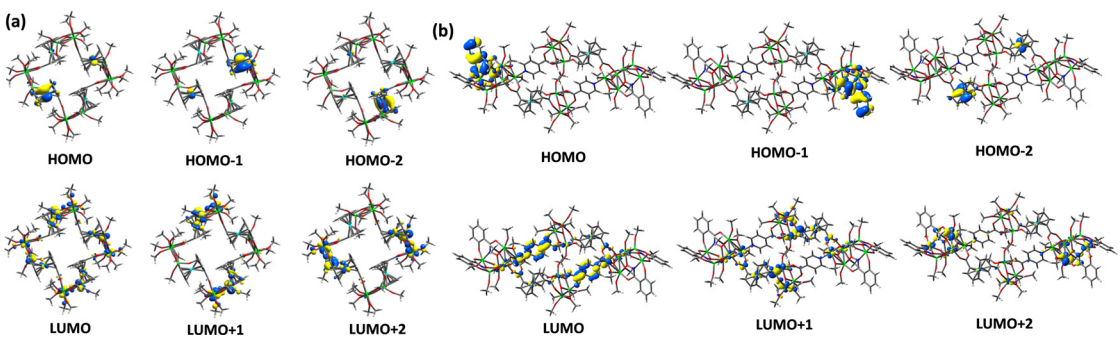

Fig. 4 Some related frontier molecular orbitals of **$Ti_{12}Fcdc_4$** (a) and **$Ti_{18}Fcdc_2$** (b).

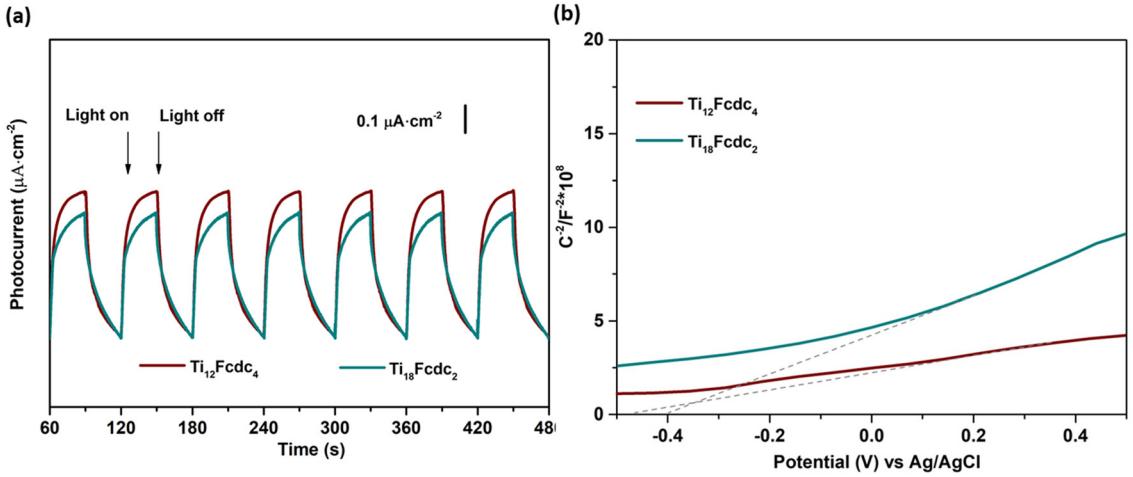

Fig. 5 (a) Photocurrent responses of $Ti_{12}Fcdc_4$ and $Ti_{18}Fcdc_2$. (b) Mott–Schottky plots of $Ti_{12}Fcdc_4$ and $Ti_{18}Fcdc_2$.

clusters containing ferrocene connectors. As shown in Fig. 5a, $Ti_{12}Fcdc_4$ and $Ti_{18}Fcdc_2$ as electrode precursors exhibit clear photocurrent responses upon on–off cycling irradiation. This rapid rise and fall in photocurrent density indicates that the carriers transport in these cluster-based materials proceeds quickly. The incorporation of $FcdcH_2$ ligands into Ti-oxo structures may effectively promote the charge transfer transition between the ferrocenyl groups and Ti-oxo cores and greatly extend the visible light absorption band, resulting in the excellent photoelectric activity of these ferrocene-sensitized titanium-oxo clusters. The photocurrent densities are 0.53 and 0.46 μA cm^{-2} for $Ti_{12}Fcdc_4$ and $Ti_{18}Fcdc_2$, respectively. The enhanced photoelectric activity of $Ti_{12}Fcdc_4$ can be mainly attributed to the broader light absorption and narrower band gap in comparison with that of $Ti_{18}Fcdc_2$. Moreover, the intrinsic structure and coordination environment of Ti-oxo clusters also directly affect their photoelectric responses. The XRD patterns and IR spectra of the samples after photocurrent measurements were basically identical to those of the original compounds, indicating that these compounds are stable during the photoelectric experiments (Fig. S5 and S6†).

Fig. 5b displays the Mott–Schottky plot. The slopes of the plots for these photoelectrodes were positive which demonstrated that $Ti_{12}Fcdc_4$ and $Ti_{18}Fcdc_2$ exhibit typical characteristics of n-type semiconductors. A lower slope was observed for $Ti_{12}Fcdc_4$ compared to that of $Ti_{12}Fcdc_4$, suggesting a higher carrier density. The corresponding flat band potential can be obtained from the interception of the plots with the potential axis. They are −0.26 V (*vs.* NHE) for $Ti_{12}Fcdc_4$ and −0.20 V (*vs.* NHE) for $Ti_{18}Fcdc_2$. For an n-type semiconductor, the flat band potential is about 0.1 eV positive than the conduction band potential. Based on the band gap, the corresponding valence band potentials are calculated to be about 1.69 and 1.81 V (*vs.* NHE) for $Ti_{12}Fcdc_4$ and $Ti_{18}Fcdc_2$, respectively. Additionally, the Nyquist plots of electrochemical impedance spectroscopy (EIS) could illustrate the interfacial charge transfer process (Fig. S12†). The radius of the arc is related to the charge transfer resistance occurring on the surface of the electrode, and the smaller radius means the higher charge transfer efficiency. Furthermore, the size of the semicircle for the $Ti_{12}Fcdc_4$ electrode is smaller than that of the $Ti_{18}Fcdc_2$ electrode, suggesting the greatly improved charge transfer efficiency. These findings are also consistent with the results of the photocurrent measurements.

Conclusions

In summary, two Ti-oxo clusters containing ferrocene connectors were successfully synthesized using {Ti_6} and/or {Ti_3} units as building blocks and $FcdcH_2$ ligands as bridging connectors. The introduction of ferrocene ligands has positive effects on the light absorption behaviors and carrier charge transfer of the resulting clusters. Moreover, these two clusters as electrode precursors showed excellent photocurrent responses under visible light irradiation, suggesting that they may have promising applications in fields such as photocurrent sensors and dye-sensitized solar cells. Further studies on the assembly engineering and photoelectric behaviors of Ti-oxo clusters containing ferrocene ligands as photosensitizers are underway.

Conflicts of interest

There are no conflicts to declare.

Acknowledgements

C. Wang acknowledges the support from the Qilu University of Technology Science Research Initial Fund.

References

1 W. H. Fang, L. Zhang and J. Zhang, Synthetic strategies, diverse structures and tuneable properties of polyoxo-titanium clusters, *Chem. Soc. Rev.*, 2018, **47**, 404–421.
2 P. Coppens, Y. Chen and E. Trzop, Crystallography and properties of polyoxotitanate nanoclusters, *Chem. Rev.*, 2014, **114**, 9645–9661.
3 L. Rozes and C. Sanchez, Titanium-oxo-clusters: precursors for a Lego-like construction of nanostructured hybrid materials, *Chem. Soc. Rev.*, 2011, **40**, 1006–1030.
4 N. Li, P. D. Matthews, H. K. Luo and D. S. Wright, Novel properties and potential applications of functional ligand-modified polyoxotitanate cages, *Chem. Commun.*, 2016, **52**, 11180–11190.
5 P. D. Matthews, T. C. King and D. S. Wright, Structure, photochemistry and applications of metal doped polyoxotitanium alkoxide cages, *Chem. Commun.*, 2014, **50**, 12815–12823.
6 Y. J. Liu, W. H. Fang, L. Zhang and J. Zhang, Recent advances in heterometallic polyoxotitanium clusters, *Coord. Chem. Rev.*, 2020, **404**, 213099.
7 Q. Y. Zhu and J. Dai, Titanium oxo/alkoxyl clusters anchored with photoactive ligands, *Coord. Chem. Rev.*, 2021, **430**, 213664.
8 U. Schubert, Titanium-Oxo Clusters with Bi- and Tridentate Organic Ligands: Gradual Evolution of the Structures from Small to Big, *Chem. – Eur. J.*, 2021, **27**, 11239–11256.
9 C. Y. Liu and Y. F. Wang, Supramolecular Chemistry of Titanium Oxide Clusters, *Chem. – Eur. J.*, 2021, **27**, 4270–4282.
10 M. Y. Fu, H. Y. Wang, H. L. Zhai, Q. Y. Zhu and J. Dai, Assembly of a Titanium-Oxo Cluster and a Bismuth Iodide Cluster, a Single-Source Precursor of a p–n-Type Photocatalyst, *Inorg. Chem.*, 2021, **60**, 9589–9597.
11 C. Zhao, Y. Z. Han, S. Dai, X. Chen, J. Yan, W. Zhang, H. Su, S. Lin, Z. Tang, B. K. Teo and N. F. Zheng, Microporous cyclic titanium-oxo clusters with labile surface ligands, *Angew. Chem., Int. Ed.*, 2017, **56**, 16252–16256.
12 Y. R. Zhao, H. Zheng, L. Q. Chen, H. J. Chen, X. J. Kong, L. S. Long and L. S. Zheng, The effect on the luminescent properties in lanthanide-titanium-oxo clusters, *Inorg. Chem.*, 2019, **58**, 10078–10083.
13 N. Li, D. Pranantyo, E. T. Kang, D. S. Wright and H. K. Luo, A simple drop-and-dry approach to grass-like multifunctional nano-coating on flexible cotton fabrics using in situ generated coating solution comprising titanium-oxo custers and silver nanoparticles, *ACS Appl. Mater. Interfaces*, 2020, **12**, 12093–12100.
14 N. Li, D. Pranantyo, E. T. Kang, D. S. Wright and H. K. Luo, In situ self-assembled polyoxotitanate cages on flexible cellulosic substrates: multifunctional coating for hydrophobic, antibacterial, and UV-blocking applications, *Adv. Funct. Mater.*, 2018, **28**, 1800345.
15 P. Yang, Z. W. Zhang, G. D. Zou, Y. Huang, N. Li and Y. Fan, Template Thermolysis to Create a Carbon Dots-Embedded Mesoporous Titanium-Oxo Sulfate Framework for Visible-Light Photocatalytic Applications, *Inorg. Chem.*, 2020, **59**, 2062–2069.
16 X. Fan, J. H. Wang, K. F. Wu, L. Zhang and J. Zhang, Isomerism in titanium-oxo clusters: molecular anatase model with atomic structure and improved photocatalytic activity, *Angew. Chem., Int. Ed.*, 2019, **58**, 1320–1323.
17 B. C. Zhu, Q. L. Hong, X. F. Yi, J. Zhang and L. Zhang, Supra-molecular co-assembly of the Ti_8L_{12} cube with $[Ti(DMF)_6]$ species and Ti_{12}-oxo cluster, *Inorg. Chem.*, 2020, **59**, 8291–8297.
18 W. H. Fang, L. Zhang and J. Zhang, A 3.6 nm Ti_{52}-oxo nanocluster with precise atomic structure, *J. Am. Chem. Soc.*, 2016, **138**, 7480–7483.
19 M. Y. Gao, F. Wang, Z. G. Gu, D. X. Zhang, L. Zhang and J. Zhang, Fullerene like polyoxotitanium cage with high solution stability, *J. Am. Chem. Soc.*, 2016, **138**, 2556–2559.
20 M. Czakler, C. Artner and U. Schubert, Two new hexanuclear titanium-oxo cluster types and their structural connection to known clusters, *New J. Chem.*, 2018, **42**, 12098–12103.
21 G. Zhang, C. Liu, D. L. Long, L. Cronin, C. H. Tung and Y. F. Wang, Water-soluble pentagonal-prismatic titanium-oxo clusters, *J. Am. Chem. Soc.*, 2016, **138**, 11097–11100.
22 Y. Z. Yu, Y. Guo, Y. R. Zhang, M. M. Liu, Y. R. Feng, C. H. Geng and X. M. Zhang, A series of silver doped butterfly-like Ti_8Ag_2 clusters with two Ag ions panelled on a Ti_8 surface, *Dalton Trans.*, 2019, **48**, 13423–13429.
23 Y. P. He, G. H. Chen, D. J. Li, Q. H. Li, L. Zhang and J. Zhang, Combining Titanium-Organic Cage and Hydrogen-Bonded Organic Cage for Highly Effective Third-Order Nonlinear Optics, *Angew. Chem.*, 2021, **133**, 2956–2959.
24 X. Fan, F. R. Yuan, D. J. Li, S. Chen, Z. B. Cheng, Z. J. Zhang, S. J. Xiang, S. Q. Zang, J. Zhang and L. Zhang, Threefold Collaborative Stabilization of Ag_{14}-Nanorods by Hydrophobic Ti_{16}-Oxo Clusters and Alkynes: Designable Assembly and Solid-State Optical-Limiting Application, *Angew. Chem., Int. Ed.*, 2021, **60**, 12949–12954.
25 Y. Y. Sun, D. F. Lu, Y. Z. Sun, Q. Wei, M. Y. Gao, N. Zheng, C. Gu, F. Wang and J. Zhang, Large Titanium-oxo Clusters as Precursors to Synthesize the Single Crystals of Ti-MOFs, *ACS Mater. Lett.*, 2021, **3**, 64–68.
26 Y. P. He, L. B. Yuan, G. H. Chen, Q. P. Lin, Q. P. Wang, L. Zhang and J. Zhang, Water Soluble and Ultra-Stable Ti_4L_6 Tetrahedron with Coordination Assembly Function, *J. Am. Chem. Soc.*, 2017, **139**, 16845–16851.
27 M. Y. Fu, H. Y. Wang, H. L. Zhai, Q. Y. Zhu and J. Dai, A Convenient Procedure for Preparing BiOX–TiO_2 Photoelectrocatalytic Electrodes from a Titanium-Oxo Compound-Modified Carbon Fiber Cloth, *Inorg. Chem.*, 2022, **61**, 4024–4032.
28 C. Y. Ge, J. L. Ho, Z. Y. Zhou, Q. Y. Zhu and J. Dai, A Cyclic Titanium-Oxo Cluster with a Tetrathiafulvalene Connector as a Precursor for Highly Efficient Adsorbent of Cationic Dyes, *Inorg. Chem.*, 2022, **61**, 486–495.

29 X. Fan, L. B. Yuan, J. Zhang and L. Zhang, Phenol-triggered supramolecular transformation of titanium–oxo cluster based coordination capsules, *Chin. Chem. Lett.*, 2021, **32**, 2415–2418.
30 Y. P. He, G. H. Chen, D. J. Li, Q. H. Li, L. Zhang and J. Zhang, Combining Titanium-Organic Cage and Hydrogen-Bonded Organic Cage for Highly Effective Third-Order Nonlinear Optics, *Angew. Chem., Int. Ed.*, 2021, **60**, 2920–2923.
31 M. Y. Gao, X. Fan, L. Zhang and J. Zhang, Dicarboxylate Ligands Oriented Assembly of $\{Ti_3(\mu_3\text{-}O)\}$ Units: From Dimer to Coordination Triangles and Rectangles, *Inorg. Chem.*, 2018, **57**, 5642–5647.
32 Q. R. Ding, G. L. Xu, L. Zhang and J. Zhang, Ligand-directed assembly engineering of trapezoidal $\{Ti_5\}$ building blocks stabilized by dimethylglyoxime, *Dalton Trans.*, 2019, **48**, 9916–9919.
33 X. X. Liu, G. H. Chen, J. Tao, J. Zhang and L. Zhang, Synthesis, Structure, and Light Absorption Behaviors of Prismatic Titanium-Oxo Clusters Containing Lacunary Lindqvist-like Species, *Inorg. Chem.*, 2022, **61**, 1385–1390.
34 M. Y. Gao, L. Zhang and J. Zhang, Acid-Controlled Synthesis of Carboxylate-Stabilized Ti_{44}-Oxo Clusters: Scaling up Preparation, Exchangeable Protecting Ligands, and Photophysical Properties, *Chem. – Eur. J.*, 2019, **25**, 10450–10455.
35 H. Fu, S. Y. Zhou, X. Fan, L. Zhang and J. Zhang, Assembly and packing models of $[Ti_6Co_{12}]$ ring based on the titanium-capped cobaltclathrochelates, *Chin. Chem. Lett.*, 2021, **32**, 923–925.
36 G. H. Chen, Y. P. He, F. P. Liang, L. Zhang and J. Zhang, A green separation process of Ag via a $Ti_4(embonate)_6$ cage, *Dalton Trans.*, 2021, **49**, 17194–17199.
37 R. Y. Chen, G. H. Chen, Y. P. He, H. Xu and J. Zhang, Synthesis and Third-Order Nonlinear Optical Properties of Metal-Organic Zeolites Built from $Ti_4(embonate)_6$ Tetrahedra, *Cryst. Growth Des.*, 2022, **22**, 66–73.
38 C. Y. Liu, C. Gao, A. Said, H. H. Niu, D. X. Wang, C. H. Tung and Y. F. Wang, Assembly of Interlocked Superstructures with a Titanium Oxide Molecular Ring in Water, *Inorg. Chem.*, 2021, **60**, 14520–14524.
39 N. Li, J. Liu, J. J. Liu, L. Z. Dong, S. L. Li, B. X. Dong, Y. H. Kan and Y. Q. Lan, Self-assembly of a phosphate-centered polyoxo-titanium cluster: discovery of the heteroatom keggin family, *Angew. Chem., Int. Ed.*, 2019, **58**, 17260–17264.
40 H. Zheng, M. H. Du, S. C. Lin, Z. C. Tang, X. J. Kong, L. S. Long and L. S. Zheng, Assembly of a wheel like $Eu_{24}Ti_8$ cluster under the guidance of high resolution electrospray ionization mass Spectrometry, *Angew. Chem., Int. Ed.*, 2018, **57**, 10976–10979.
41 C. Y. Liu, J. Y. Hu, W. M. Liu, F. Zhu, G. Wang, C. H. Tung and Y. F. Wang, Binding Modes of Salicylic Acids to Titanium Oxide Molecular Surfaces, *Chem. – Eur. J.*, 2020, **26**, 2666–2674.
42 C. Y. Liu, J. Y. Hu, F. Zhu, J. H. Zhan, L. Du, C. H. Tung and Y. F. Wang, Functionalization of Titanium Oxide Cluster $Ti_{17}O_{24}(O^iC_3H_7)_{20}$ with Catechols: Structures and Ligand-Exchange Reactivities, *Chem. – Eur. J.*, 2019, **25**, 14843–14849.
43 D. H. Zou, L. N. Cui, P. Y. Liu, S. Yang, Q. Y. Zhu and J. Dai, Molecular model of dye sensitized titanium oxides based on aryl-amine dye anchored titanium-oxo clusters, *Inorg. Chem.*, 2019, **58**, 9246–9252.
44 J. L. Hou, Y. G. Weng, P. Y. Liu, L. N. Cui, Q. Y. Zhu and J. Dai, Effects of the ligand structures on the photoelectric activities, a model study based on titanium-oxo clusters anchored with S-heterocyclic ligands, *Inorg. Chem.*, 2019, **58**, 2736–2743.
45 L. N. Cui, P. Y. Liu, L. Yang, X. P. Shu, Q. Y. Zhu and J. Dai, A series of Ti_6-oxo clusters anchored with arylamine dyes: effect of dye structures on photocurrent responses, *Chem. – Asian J.*, 2019, **14**, 3198–3204.
46 Q. R. Ding, Y. H. Yu, C. S. Cao, J. Zhang and L. Zhang, Stepwise assembly and reversible structural transformation of ligated titanium coated bismuthoxo cores: shell morphology engineering for enhanced chemical fixation of CO_2, *Chem. Sci.*, 2022, **13**, 3395–3401.
47 Y. H. Guo, Y. Z. Yu, Y. H. Shen, L. G. Yang, N. N. Liu, Z. Y. Zhou and Y. S. Niu, "Three-in-One" Structural-Building-Mode-Based Ti_{16}-Type Titanium Oxo Cluster Entirely Protected by the Ligands Benzoate and Salicylhydroxamate, *Inorg. Chem.*, 2022, **61**, 8685–8693.
48 Q. R. Ding, Y. H. Yu, C. S. Cao, J. Zhang and L. Zhang, Stepwise assembly and reversible structural transformation of ligated titanium coated bismuthoxo cores: shell morphology engineering for enhanced chemical fixation of CO_2, *Chem. Sci.*, 2022, **13**, 3395–3401.
49 H. Y. Wang, M. Y. Fu, H. L. Zhai, Q. Y. Zhu and J. Dai, Mono- and Bismetalphenanthroline-Substituted Ti_{12} Clusters: Structural Variance and the Effect on Electronic State and Photocurrent Property, *Inorg. Chem.*, 2021, **60**, 12255–12262.
50 R. Gao, S. M. Chen, F. Wang and J. Zhang, Single-Crystal Syntheses and Properties of Indium-Organic Frameworks Based on 1,1′-Ferrocenedicarboxylic Acid, *Inorg. Chem.*, 2021, **60**, 239–245.
51 J. Benecke, E. S. Grape, A. Fuß, S. Wöhlbrandt, T. A. Engesser, A. K. Inge, N. Stock and H. Reinsch, Polymorphous Indium Metal-Organic Frameworks Based on a Ferrocene Linker: Redox Activity, Porosity, and Structural Diversity, *Inorg. Chem.*, 2020, **59**, 9969–9978.
52 Q. X. Wang, Z. C. Guo, Y. Qin, X. Wang and G. Li, High Proton Conduction in Three Highly Water-Stable Hydrogen-Bonded Ferrocene-Based Phenyl Carboxylate Frameworks, *Inorg. Chem.*, 2021, **60**, 19278–19286.
53 Z. K. Huang, H. J. Yu, L. Wang, X. W. Liu, T. F. Lin, F. Haq, S. Z. Vatsadze and D. A. Lemenovskiy, Ferrocene-contained metal organic frameworks: From synthesis to applications, *Coord. Chem. Rev.*, 2021, **430**, 213737.

54 J. L. Hou, W. Luo, Y. Guo, P. Zhang, S. Yang, Q. Y. Zhu and J. Dai, Titanium Oxo Cluster with Six Peripheral Ferrocene Units and Its Photocurrent Response Properties for Saccharides, *Inorg. Chem.*, 2017, **56**, 6451–6458.

55 Y. Fan, H. M. Li, R. H. Duan, H. T. Lu, J. T. Cao, G. D. Zou and Q. S. Jing, Phosphonate-Stabilized Titanium-Oxo Clusters with Ferrocene Photosensitizer: Structures, Photophysical and Photoelectrochemical Properties, and DFT/TDDFT Calculations, *Inorg. Chem.*, 2017, **56**, 12775–12782.

56 Z. C. Liu, J. Y. Lei, M. Frasconi, X. H. Li, D. Cao, Z. X. Zhu, S. T. Schneebeli, G. C. Schatz and J. F. Stoddart, A Square-Planar Tetracoordinate Oxygen-Containing Ti_4O_{17} Cluster Stabilized by Two 1,1′-Ferrocenedicarboxylato Ligands, *Angew. Chem., Int. Ed.*, 2014, **53**, 9193–9197.

57 J. J. Liu, N. Li, J. W. Sun, J. Liu, L. Z. Dong, S. J. Yao, L. Zhang, Z. F. Xin, J. W. Shi, J. X. Wang, S. L. Li and Y. Q. Lan, Ferrocene-Functionalized Polyoxo-Titanium Cluster for CO_2 Photo-reduction, *ACS Catal.*, 2021, **11**, 4510–4519.

58 E. M. Han, W. D. Yu, L. J. Li, X. Y. Yi, J. Yan and C. Liu, Accurate assembly of ferrocene-functionalized $\{Ti_{22}Fc_4\}$ clusters with photocatalytic amine oxidation activity, *Chem. Commun.*, 2021, **57**, 2792–2795.